PHYSICAL REVIEW A VOLUME 4, NUMBER 4 OCTOBER 1971

# Differential and Integral Cross Sections for the Electron-Impact Excitation of the $a\,^1\Delta_g$ and $b\,^1\Sigma_g^+$ States of $O_2$

S. Trajmar*
*California Institute of Technology, Jet Propulsion Laboratory, Pasadena, California* 91103

and

D. C. Cartwright†
*Space Physics Laboratory, The Aerospace Corporation, El Segundo, California* 90245

and

W. Williams*
*California Institute of Technology, Jet Propulsion Laboratory, Pasadena, California* 91103
(Received 1 April 1971)

Electron-impact energy-loss spectra of $O_2$ have been analyzed for incident electron energies from 4 to 45 eV, scattering angles from 10° to 90°, and energy losses from 0 to 5 eV. The inelastic processes observed were the excitation of the $a\,^1\Delta_g$ and $b\,^1\Sigma_g^+$ electronic states and vibrational excitation in some cases to $v''=13$. The excitation cross sections at each energy were made absolute by normalizing the sum of the integral cross sections (all inelastic, ionization, and elastic) to measured electron-$O_2$ total cross sections. The differential cross sections for the $a\,^1\Delta_g$ and $b\,^1\Sigma_g^+$ states show nearly isotropic behavior, as expected for optically spin-forbidden transitions. The elastic differential cross sections are strongly forward peaked at higher energies, but become only slightly forward peaked at the lower energies. The integral cross sections for the excitation of the $a\,^1\Delta_g$ and $b\,^1\Sigma_g^+$ states reach their maxima near 7 eV and are more than an order of magnitude larger than previous estimates. The integral elastic cross section reaches its maximum at around 10 eV.

## I. INTRODUCTION

Molecular oxygen plays an important role in the physics and chemistry of the earth's atmosphere. The need for accurate electron-impact cross sections for excitation of the $a\,^1\Delta_g$ and $b\,^1\Sigma_g^+$ states became apparent with the observation[1] of the intense auroral emission at 1.27 $\mu$ resulting from the $a\,^1\Delta_g$ $(v'=0)\rightarrow X\,^3\Sigma_g^-(v''=0)$ transition. Subsequent measurements in auroras[2] and in the disturbed ionosphere[3] indicate that electron impact plays an important role in the population of these lower electronic states of $O_2$. Knowledge of the electron-impact cross sections for these low-lying electronic states is not only important for the study of the infrared emissions from $O_2$, but also necessary in order to understand other processes taking place in the ionosphere which result from the population of these states.

Very few measurements of these excitation cross sections have been reported. Schulz and Dowell[4] placed upper limits on the integral cross sections for excitation of the $a\,^1\Delta_g$ and $b\,^1\Sigma_g^+$ states of $3\times10^{-20}$ and $6\times10^{-21}$ cm$^2$, respectively, in the threshold energy region by measurements using the trapped-electron method. Hasted[5] studied both the vibrational and the $a\,^1\Delta_g$ excitation processes by electron impact at 0° scattering angle and at impact energies below about 2 eV. He found no $a\,^1\Delta_g$ excitation and concluded that the cross section for this process is less than 10% of the $(v''=0\rightarrow v''=1)$ vibrational excitation cross section. Skerbele *et al.*[6] measured the angular distribution of electrons scattered into the 0°–16° region after excitation of the $a\,^1\Delta_g$ state at an incident energy of 45 eV, but have reported no measurements at lower impact energies or larger scattering angles. Watson *et al.*[7] estimated the magnitude and shape of the total excitation cross sections to the $a\,^1\Delta_g$ and $b\,^1\Sigma_g^+$ states by making assumptions concerning the similarity of these excitations to other exchange processes with known cross sections and by normalizing the cross-section curves to Hake and Phelps's[8] excitation functions. Recently, Konishi *et al.*[9] reported integral excitation cross sections for the $a\,^1\Delta_g$ and the $b\,^1\Sigma_g^+$ states in the 20–70-eV impact energy range.

Experimental differential and integral cross sections for electron-impact excitation of the $a\,^1\Delta_g$ and $b\,^1\Sigma_g^+$ states are reported here[10] for incident energies ranging from near threshold to 45 eV. The experimental methods and the technique used to analyze the data are briefly discussed and a comparison with the previous values for these cross sections is made.

## II. EXPERIMENTAL

The electron-impact spectrometer which was used to carry out these measurements has been described in detail elsewhere[11,12] and is shown schematically in Fig. 1. The sensitivity of the apparat-

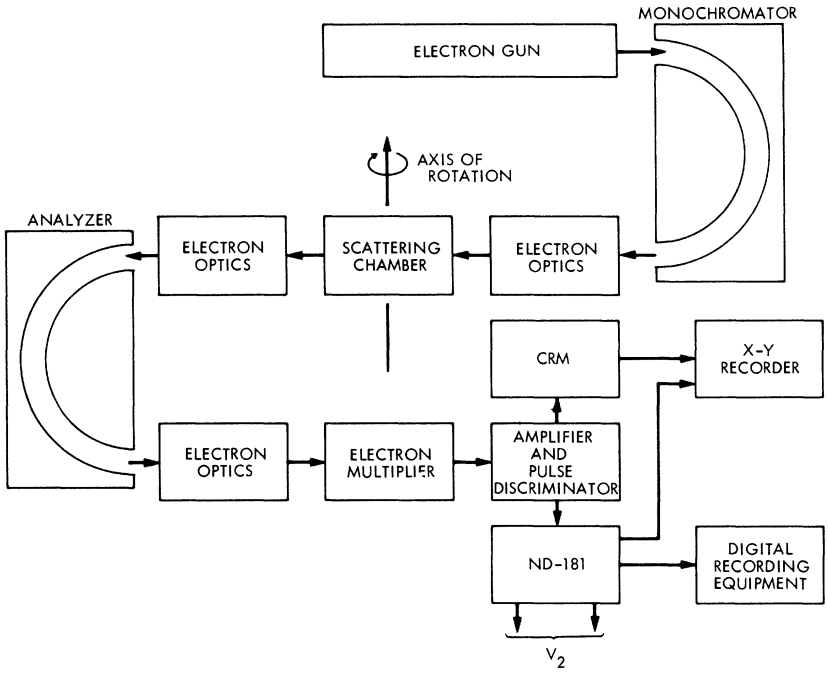


FIG. 1. Schematic diagram of apparatus. The block labeled ND-181 represents the nuclear data model ND-181 1024 channel scaler whose analog output voltage ($V_2$) is used to sweep the energy-loss (or impact energy) scale.

us and the signal-to-noise ratio were recently improved by the introduction of new electron optics and a channeltron electron multiplier.

The experimental data were obtained by scattering an energy-selected electron beam (energy $E$) off gaseous $O_2$ at about $10^{-3}$-Torr pressure. During these experiments, the full width at half-maximum (FWHM) of the elastic feature was maintained at about 0.080 eV. The scattered intensity as a function of energy loss was measured by collecting the electrons entering a small solid angle (approximately $10^{-3}$ sr) at a fixed scattering angle $\theta$. The scattering angle could be varied from $-30°$ to $+90°$. The true zero scattering angle was determined by locating the precise symmetry point of the scattering intensity for an inelastic feature in the neighborhood of the nominal zero.

The incident energy scale was calibrated by introducing a mixture of He and $O_2$ into the scattering chamber. The elastic signal ($\Delta E = 0$) was monitored at 40° as a function of impact energy and the location of the 19.31-eV He resonance was determined with respect to our own impact energy scale. The difference between 19.31 eV and our digital voltmeter reading for the He resonance was attributed to contact potentials. It was found that the contact potential determined this way varied somewhat with the pressure and with the He-to-$O_2$ ratio but never exceeded 0.050 V. We believe, therefore, that the impact energies are correct to within 0.050 eV. Similar experiments with $N_2$ and He led us to the same conclusion. The pressure was measured with an uncalibrated ion gauge and consequently our pressure readings were only approximate. However, it has been determined that at these pressures ($\sim 10^{-3}$ Torr) multiple scattering effects are negligible.

Typical energy-loss spectra are shown in the upper portions of Figs. 2–5. These spectra are the superposition of many repetitive scans obtained with a 1024 channel scaler. The memory advance in the scaler generated analog voltage steps which were used to sweep the energy-loss scale. The spectrum from the scaler memory was transferred to IBM cards and/or tape for subsequent computer manipulation.

It generally takes several days of continuous operation to obtain energy-loss spectra over the entire angular range at any one incident energy. During this period, it is likely that the experimental conditions will have changed and as a result the energy-loss spectra obtained at one scattering angle cannot be directly compared to those at a different scattering angle. However, the relative intensities within one energy-loss spectrum are not subject to experimental errors associated with changing instrumental conditions because the duration of a single scan is short compared to the rate of these changes and each spectrum is the result of many scans. The measured relative intensities are equal to the ratios of the respective differential cross sections (DCS's) if the effective-path-length corrections (EPLC) for the two transitions concerned are the same. This is the case in the present measurements for scattering angles >10°.

The procedure for determining the cross section

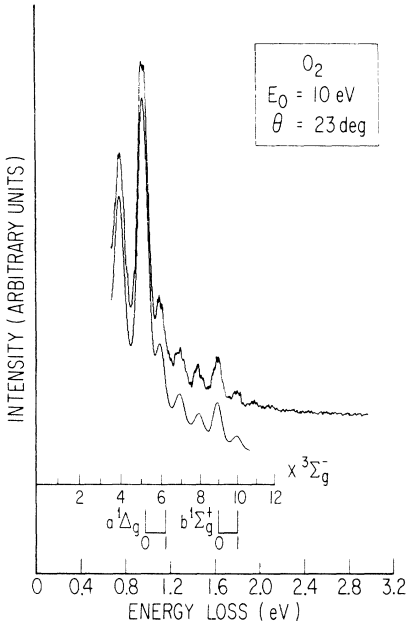


FIG. 2. Electron-impact energy-loss spectrum at $E$ = 10 eV, $\theta$=23°. The upper curve is the experimental spectrum and the lower one is the computer-synthetized spectrum, which has been shifted down for clarity of presentation. The energy-loss location of the vibrational levels of the $X^3\Sigma_g^-$, $a^1\Delta_g$, and $b^1\Sigma_g^+$ states are indicated in the lower portion of the figure.

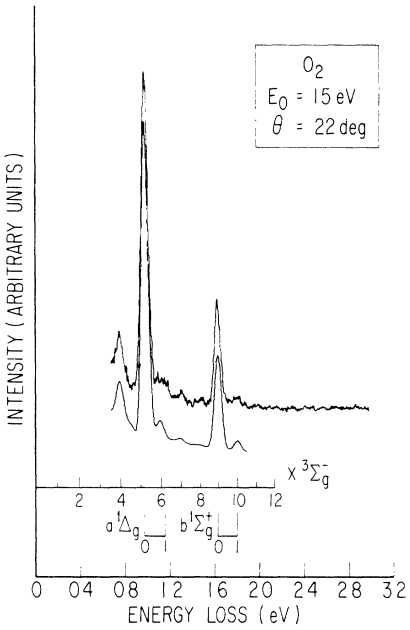


FIG. 4. Same as Fig. 2 except $E$ = 15 eV and $\theta$ = 22°.

was as follows. A spectrum including the elastic and inelastic features was obtained at each $E$ and $\theta$. From these spectra the *ratios* of the inelastic scattering intensities to the elastic intensity were determined by procedures to be discussed in Secs. III A and III B. From these ratios and the elastic DCS, the inelastic DCS's were obtained in the same arbitrary units, and the normalization to the absolute scale was carried out as described in Sec. III C.

The elastic DCS was obtained as follows. At each

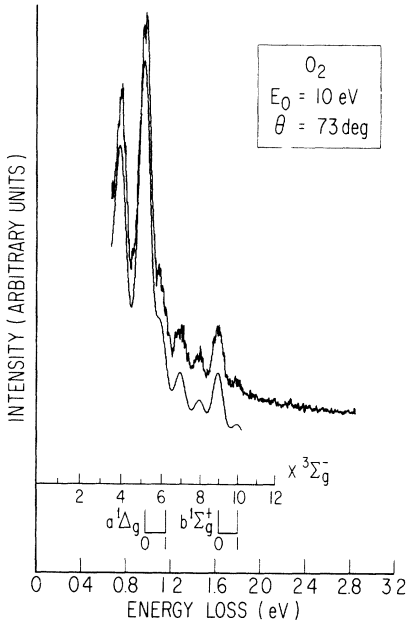


FIG. 3. Same as Fig. 2 except $\theta$=73°.

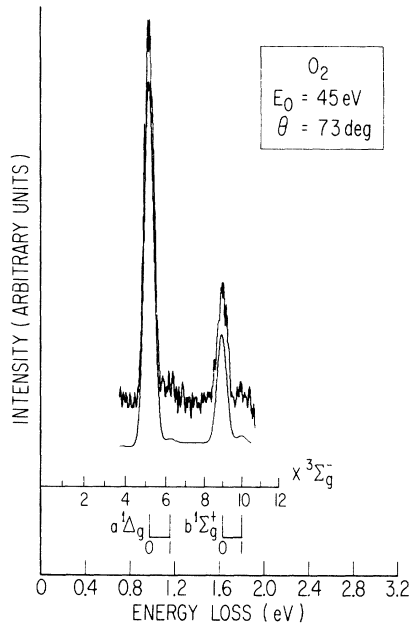


FIG. 5. Same as Fig. 2 except $E$ = 45 eV.

incident energy the elastic scattering intensity was measured as a function of angle under constant instrumental conditions (this required about 1 h). To these intensities an EPLC was applied to correct for the change in scattering geometry with scattering angle and thereby obtain the elastic DCS in arbitrary units. The elastic intensity could not be accurately measured for scattering angles $< 10°$ with the present apparatus due to direct beam interference and saturation of the counting apparatus. Consequently, the inelastic features could not be normalized to the elastic DCS below 10°. For this angular region, the inelastic features were calibrated, relative to the $X\,^3\Sigma_g^-\,(v''=0) \rightarrow a\,^1\Delta_g(v'=0)$ feature, down to 0° by using the fact that for energy losses greater than a few tenths of an eV, the analyzer eliminates the direct beam interference. To the low-angle intensity curves an EPLC was applied and the resulting curves were then normalized to the ones obtained from the intensity ratios at the region of overlap (usually 15° – 30°). Low-angle calibrations down to 5° were carried out at 7, 10, and 20 eV for $a\,^1\Delta_g$ and at 10, 15, and 20 eV for the $b\,^1\Sigma_g^+$ transitions. At the other impact energies the curves were extrapolated below 10°, using judgement aided by the three low-angle calibrations. Although the scattering intensities so obtained are as reliable as at higher angles, the resulting DCS's have a somewhat larger uncertainty at low angles because of the larger uncertainties in the EPLC. The EPLC is a more sensitive function of the scattering geometry and of the DCS itself at low angles than at high ones. Effective scattering path length corrections were calculated with varying scattering geometry and DCS angular behaviors, and our conclusion is that the EPLC did not introduce more than 10% error into the low-angle DCS's reported here.

## III. DATA ANALYSIS

### A. Least-Squares Technique

The magnitude of each inelastic feature present in the energy-loss spectrum can be extracted by application of a computer least-squares technique as follows. The energy levels and Franck-Condon factors connecting each vibrational level of each excited electronic state with the lowest vibrational level of the ground electronic state are assumed to be known while the intensities of the various inelastic features present in each spectrum are to be determined. The rotationally averaged[13] DCS for excitation of vibrational level $v'$ of electronic state $n'$ at incident energy $E$ and scattering angle $\theta$ is denoted by $\sigma_{n'v'}(E, \theta)$. The scattered electron current at energy loss $W$ for an "ideal" measuring system of nearly perfect resolution is related to the total number of electronic transitions $N$, containing $M(n')$ vibrational bands, by

$$I_m(E, \theta, W', \rho, I_0) = I_0 C(E,\theta) \sum_{n'=0}^{N} \sum_{v'=0}^{M(n')} \rho \sigma_{n'v'}(E, \theta) \times g_{n'v'}(W' - W_{n'v'}) , \quad (1)$$

where $I_m(E, \theta, W', \rho, I_0)$ is the number of scattered electrons per second per steradian at impact energy $E$, scattering angle $\theta$, and energy loss $W'$ from a target gas of density $\rho$. The quantity $I_0$ is the incident beam intensity (number of electrons per second), and $C(E, \theta)$ is a constant at a given impact energy which incorporates the effective-path-length correction and all instrument efficiency factors. The natural line shape of the $n''v'' \rightarrow n'v'$ transition is characterized by $g_{n'v'}(W' - W_{n'v'})$.

In practice, the energy-loss spectra are affected by resolution properties of the experimental apparatus such that the actual signal $S$ is given by

$$S(E, \theta, W, \rho, I_0) = \int_{-\infty}^{\infty} I_m(E, \theta, W', \rho, I_0) F(W' - W) dW' , \quad (2)$$

where $F(W' - W)$ is a function which characterizes the effective resolution of the measuring device. In the work reported here the natural line shape is so much narrower than the line shape produced by the analyzer, that $g_{n'v'}$ can effectively be treated as a $\delta$ function in $W'$ space. Equations (1) and (2) can then be combined and the integration over $W'$ done immediately to give

$$S(E, \theta, W, \rho, I_0) = I_0 C(E, \theta) \rho \sum_{n'=0}^{N} \sum_{v'=0}^{M(n')} \sigma_{n'v'}(E, \theta) \times F(W_{n'v'} - W) . \quad (3)$$

Within the framework of the Born-Oppenheimer nuclear-electronic mass-separation approximation, the relative vibrational intensities are independent of incident energy and scattering angle so that $\sigma_{n'v'}$ can be written as

$$\sigma_{n'v'}(E, \theta) = \sigma_{n'}(E, \theta) q_{v'v''} , \quad (4)$$

where $q_{v'v''}$ is the Franck-Condon factor and $\sigma_{n'}$ now contains all the information concerning the angular dependence and absolute value of the DCS for a given electronic transition. Substituting Eq. (4) into Eq. (3), the scattered intensity becomes

$$S(E, \theta, W, \rho, I_0) = I_0 C(E, \theta) \rho \sum_{n'=0}^{N} \sigma_{n'}(E, \theta) \sum_{v'=0}^{M(n')} q_{v'v''} \times F(W_{n'v'} - W) + B(E, \theta, W, \rho, I_0) , \quad (5)$$

where $B(E, \theta, W, \rho, I_0)$ represents any background contribution to the measured signal. One notes that because of the unknown factor $I_0 \rho C(E)$ which appears in the above equations, the $\sigma_{n'}$ obtained for one incident energy cannot be directly compared to that measured at a different incident energy. The absolute calibration of these DCS's obtained

at different incident energies will be discussed in Sec. III C.

During the time required to accumulate a spectrum, $I_0$ and $\rho$ remain constant and in all cases encountered so far, the background is well represented by the form

$$B(E, \theta, W) = \sum_{i=1}^{L} a_i(E, \theta) h_i(W) , \tag{6}$$

where the $h_i$ are known functions of the energy loss and the coefficients $a_i(E, \theta)$ are to be determined.

The quantities $X_{n'}(E, \theta) \equiv I_0 \rho C(E, \theta) \sigma_{n'}(E, \theta)$ and $a_i(E, \theta)$ are determined for a given resolution in each spectrum from Eqs. (5) and (6) by requiring that the difference between the measured and calculated spectrum be a minimum in a least-squares sense. That is, if $S_M(E, \theta, W)$ is the measured signal, then the quantity

$$\epsilon = \sum_{j=1}^{D} (S_M - S)^2 \tag{7}$$

is minimized, where $D$ is the number of data points and $S$ is as defined in Eq. (5). The canonical equations to be solved are obtained from (7) as

$$\begin{aligned} &\frac{\partial \epsilon}{\partial X_{n'}} = 0 , \qquad n' = 1, \ldots, N \\ &\frac{\partial \epsilon}{\partial a_i} = 0 , \qquad i = 1, \ldots, L \end{aligned} \tag{8}$$

and represent a set of $N+L$ linear algebraic equations, the solution of which are the unknown coefficients $X_{n'}$ and $a_i$. With these coefficients, the scattered signal intensities at the channels corresponding to the peak position of the inelastic features are calculated. These calculated intensities are then divided by the elastic peak intensity appearing in the same spectrum to yield the intensity ratios at each scattering angle and incident energy.

### B. $O_2$ Analysis

Each energy-loss spectrum acquired at fixed incident energy and scattering angle consisted of either 512 or 1024 channels of intensity points taken in steps of about 4 or 2 mV, respectively. These data were then smoothed by averaging the signal over three neighboring channels to remove some of the noise which was present in the measurements. The vibrational energy levels and Franck-Condon factors for the $X\,^3\Sigma_g^-$, $a\,^1\Delta_g$, and $b\,^1\Sigma_g^+$ electronic states were calculated by utilizing an RKR procedure followed by direct numerical integration of the differential equation describing the molecular vibration.[14] The spectroscopic constants for these states were provided by Albritton *et al.*[15] and represent a reevaluation of all the spectroscopic data available for these states. Table I gives the excitation energies, relative to the $v''=0$ level of the ground electronic state, and the Franck-Condon factors for transitions to each vibrational level of the $a\,^1\Delta_g$ and $b\,^1\Sigma_g^+$ states.

The best fit to the measured spectra using the technique outlined in Sec. III A was accomplished as follows. The experimental resolution function $F(W_{n'v'} - W)$ was taken to be Gaussian,

$$F(x) = \frac{1}{\Delta\sqrt{\pi}} \exp\left(-\frac{x^2}{\Delta^2}\right) , \tag{9}$$

and $\Delta$ (the FWHM) was initially estimated from the experimentally measured elastic feature. The precise location of one strong inelastic feature to be used as a reference peak for each spectrum was then determined by variation of the reference peak channel in the neighborhood of the one calculated from the spectroscopic constants and from the location of the elastic peak. In the data reported here the reference peak was taken as $a\,^1\Delta_g(v'=0)$ and the precise channel for this state was determined for each spectrum as that which minimized the root-mean-square (rms) error for fixed FWHM. The reference peak determined in this fashion was always within one or two channels of that calculated from the spectroscopic data and the location of the elastic peak. With this reference peak held fixed, the FWHM was then varied until a minimum rms error was obtained for which the best least-squares fit to the input spectrum was assumed to have been found.

Examples of the input data to such a procedure and the resulting optimum computer fits are shown (as the upper and lower curves, respectively) in Figs. 2–5 for the incident energies and scattering angles indicated on the figures. The background in all spectra was taken of the form

$$B(E, \theta, W) = \sum_{i=1}^{3} a_i(E, \theta) W^{-1} . \tag{10}$$

TABLE I. Excitation energies and Franck-Condon factors for vibrational levels of the $X\,^3\Sigma_g^-$, $a\,^1\Delta_g$, and $b\,^1\Sigma_g^+$ states of $O_2$ relative to $v''=0$.

| $X\,^3\Sigma_g^-$ | | $a\,^1\Delta_g$ state | | | $b\,^1\Sigma_g^+$ state | | |
|---|---|---|---|---|---|---|---|
| $v''$ | $\Delta E$(eV) | $v'$ | $\Delta E$ | $q_{v'0}$ | $v'$ | $\Delta E$ | $q_{v'0}$ |
| 0 | 0.000 | 0 | 0.977 | 0.9869 | 0 | 1.627 | 0.9307 |
| 1 | 0.193 | 1 | 1.161 | 0.0130 | 1 | 1.801 | 0.0666 |
| 2 | 0.383 | | | | | | |
| 3 | 0.570 | | | | | | |
| 4 | 0.754 | | | | | | |
| 5 | 0.936 | | | | | | |
| 6 | 1.114 | | | | | | |
| 7 | 1.290 | | | | | | |
| 8 | 1.463 | | | | | | |
| 9 | 1.633 | | | | | | |
| 10 | 1.801 | | | | | | |
| 11 | 1.965 | | | | | | |
| 12 | 2.127 | | | | | | |

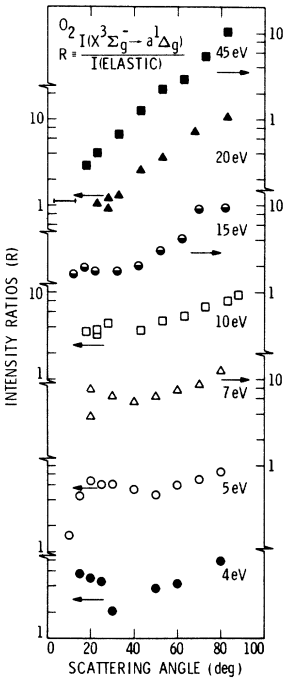


FIG. 6. Ratio of the scattering intensity of the $a\,^1\Delta_g$ excitation to that for elastic scattering, as a function of scattering angle for different impact energies. All values on the ordinate are to be multiplied by $10^{-3}$. [The line between 3° and 12° represents the 20-eV data of the Skerbele *et al.* determination (Ref. 6)].

As evident from Figs. 2–5, this computer analysis technique is a useful method of unfolding the typical spectrum obtained in energy-loss experiments.[16]

Pure vibrational excitation of the ground electronic state was observed up to $v'' = 12$ at 10 eV impact energy as can be seen in Fig. 2. In an effort to detect the presence of any resonance state which preferentially decays into only one or two vibrational levels of the ground electronic state, each $v''$ level was treated independently. Although the spectra analyzed for the $a\,^1\Delta_g$ and $b\,^1\Sigma_g^+$ cross sections do provide some evidence indicating an increased population of the higher $v''$ levels for incident energies near 10 eV, the results are not conclusive and these processes will require additional detailed examination in order to ellucidate their true energy dependence. This work is in progress and the results of this investigation as well as the vibrational excitation cross sections will be reported in a subsequent publication.[17]

### C. Absolute Calibration

From the computer analysis and procedures described above, the ratios of the inelastic to elastic scattering intensities were obtained. Figures 6 and 7 show these ratios for the $a\,^1\Delta_g$ and $b\,^1\Sigma_g^+$ excitations, respectively, at incident energies of 4, 5, 7, 10, 15, 20, and 45 eV. Using the elastic DCS's and these ratios, the DCS for each inelastic feature (in arbitrary units) was obtained. These DCS's were then extrapolated to 0° and 180° in order to obtain the angular dependence over the entire range. Because of the low-angle calibration discussed above, and because of the weighting factor in the angular integration, the extrapolation to 0° does not introduce more than about 2% error into the integral cross sections. The accuracy of the extrapolation to 180° is more difficult to assess because so little information is presently available concerning the behavior of the DCS for these types of transitions at large scattering angles. Nonetheless, an extrapolation to 180° was necessary if an estimate of the total excitation cross sections was to be obtained. Therefore a number of different forms for the large-angle extrapolation were tried in order to bracket the error in the total cross sections introduced by such extrapolation procedures. In Figs. 8–10 are displayed the absolute DCS's for elastic scattering and for the $a\,^1\Delta_g$ and $b\,^1\Sigma_g^+$ excitations, respectively, at incident energies ranging from 4 to 45 eV. The extrapolated portions of the curves are represented by broken lines while the solid portions of the DCS's are lines drawn smoothly between the data points which have been included in Figs. 9 and 10.

The elastic data points are not shown because the measurements have been repeated many times with very good reproducibility. The integral and differential cross sections were normalized by using the total scattering cross-section measurements of Salop and Nakano[18] in the incident energy range 4–20 eV and Sunshine *et al.*[19] at 45 eV. Since the total scattering cross section at any incident energy is the sum of the elastic cross section and all inelastic processes which are energetically possible, the magnitudes of all inelastic processes

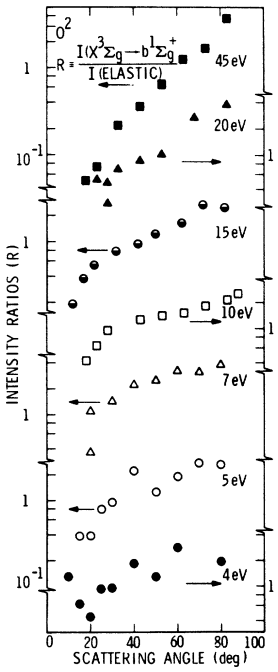


FIG. 7. Ratio of the scattering intensity of the $b\,^1\Sigma_g^+$ excitation to that for elastic scattering, as a function of scattering angle for different impact energies. All values on the ordinate are to be multiplied by $10^{-3}$.

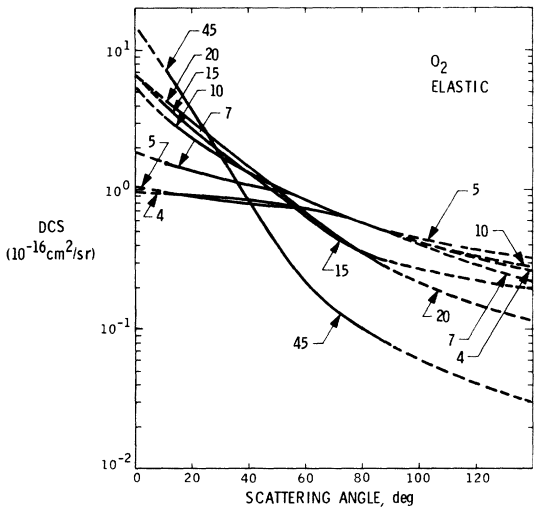


FIG. 8. Elastic differential cross sections for different incident electron energies. The incident energy in eV is indicated adjacent to the appropriate curve.

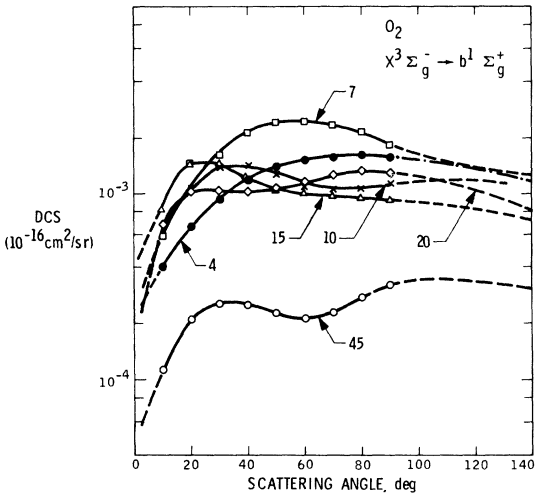


FIG. 10. Differential cross section for excitation of the $b\,^1\Sigma_g^+$ state. The incident energy in eV is indicated adjacent to the appropriate curve.

must be known in order to extract the elastic scattering cross section from total scattering measurements. As the incident energy increases, more inelastic processes become possible and the estimation of the inelastic component to the total scattering becomes increasingly difficult because all but the ionization cross section for $O_2$ are unknown.[20] In this study, the inelastic contribution to the total scattering was obtained at each energy of interest by analyzing the entire energy-loss spectra for each inelastic feature which was present, in a manner analogous to that described above for the $a\,^1\Delta_g$ and $b\,^1\Sigma_g^+$ excitations. The magnitudes of the inelastic cross sections, assumed to be present in the measured total scattering cross section, are given in Table II along with the magnitude of the elastic integral cross section used in this study. The theoretical elastic integral cross section predicted by Fisk[21] is included in the table for comparison purposes.

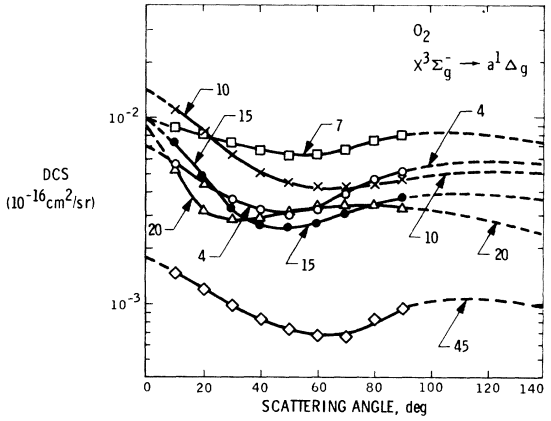


FIG. 9. Differential cross section for excitation of the $a\,^1\Delta_g$ state. The incident energy in eV is indicated adjacent to the appropriate curve.

### D. Error Analysis

The major sources of error which result in uncertainty in the integral cross sections are itemized below, and the magnitudes of the different errors are collected in Tables III and IV for the $a\,^1\Delta_g$ and $b\,^1\Sigma_g^+$ states, respectively. The percent error associated with the absolute elastic cross sections is obtained by adding the values in the last two rows at each energy.

*a. Statistical.* Since the magnitudes of the inelastic features above the background were deter-

TABLE II. Magnitudes of the inelastic cross sections present in the total scattering cross section for the incident energies used in this study. (Cross sections in units of $10^{-16}$ cm$^2$.)

| $E$(eV) | $Q_{tot}$ | $Q_{Ion}$ [a] | $\sum Q_{electr}$ [b] | $\sum Q_{vibr}$ [b] | $Q_{elastic}$ Deduced[b] | $Q_{elastic}$ Fisk[c] |
|---|---|---|---|---|---|---|
| 4 | 6.86[d] | • • • | $0.07_5$ | $0.00_7$ | 6.78 | 6.69 |
| 5 | 7.10[d] | • • • | $0.08_2$ | $0.07_0$ | 6.95 | 7.33 |
| 7 | 8.02[d] | • • • | $0.11_2$ | $0.30_4$ | 7.60 | 8.48 |
| 10 | 9.76[d] | • • • | $0.30_2$ | $0.43_3$ | 9.03 | 9.76 |
| 15 | 9.51[d] | $0.08_5$ | $1.47_6$ | $0.06_0$ | 7.89 | 9.94 |
| 20 | 9.40[d] | $0.30_7$ | $1.06_0$ | $0.00_8$ | 8.02 | 9.65 |
| 45 | 9.3[e] | 1.70 | $1.77_8$ | $0.00_8$ | 5.82 | • • • |

[a] D. Rapp and P. Englander-Golden, J. Chem. Phys. 43, 1464 (1965).
[b] This work.
[c] Reference 21.
[d] Reference 18.
[e] Reference 19.

mined by a least-squares analysis of each energy-loss spectra, the rms deviation of the computed from the measured spectrum was used as a measure of the statistical error in the experimental data. The rms deviations for each scattering angle were averaged and combined with typical values of the DCS of each electronic state to obtain the entries given in Tables III and IV.

*b. Extrapolation of inelastic* DCS *curves.* As mentioned above, the extrapolation of the DCS to 0° is fairly reliable for purposes of obtaining the total cross section since the small angles (below 10°) contribute very little to the total cross section at any single energy. However, the extrapolation from 85° to 180° is a good deal more uncertain because not only is the extrapolation range fairly large, but very little is known about the large-angle behavior of the DCS's for these types of transitions. Consequently, the best that could be done was to try a number of different large-angle extrapolation schemes which are realistic but yet sufficiently different to permit a reasonable estimate of the potential error introduced by this somewhat arbitrary extrapolation. The extrapolations used to calculate the integral cross sections are shown in Figs. 8–10. The extrapolation of the $b\,^1\Sigma_g^+$ DCS for energies < 7 eV has greater uncertainty because good data were difficult to acquire for this transition at low incident energies.

*c. Elastic.* The error introduced in the integral elastic cross section by the extrapolation to large angles is believed to be negligible due to the strong forward peaking of the elastic DCS. The errors associated with the determination of the angular distribution of the elastic scattering intensity and the subsequent effective-path-length correction are the errors listed under this heading.

*d. Normalization.* Because no experimental integral elastic cross section has been reported,[20] the magnitude of this cross section was obtained from total scattering measurements as outlined above. The estimated error, which depends on the incident energy, reflects the uncertainty in determining the magnitudes of the various inelastic processes which can contribute to the total scattering cross section.

TABLE III. Estimated percent errors in the integral cross section for $a\,^1\Delta_g$.

| Type error \ $E$(eV) | 4 | 5 | 7 | 10 | 15 | 20 | 45 |
|---|---|---|---|---|---|---|---|
| Statistical | 10 | 5 | 6 | 5 | 5 | 10 | 10 |
| Extrapolation | 5 | 4 | 10 | 5 | 7 | 10 | 15 |
| Elastic DCS | 7 | 7 | 5 | 4 | 4 | 4 | 2 |
| Normalization | 3 | 5 | 4 | 10 | 4 | 10 | 15 |
| Total (%) | 25 | 21 | 25 | 24 | 20 | 34 | 42 |

TABLE IV. Estimated percent errors in the integral cross section for $b\,^1\Sigma_g^+$.

| Type error \ $E$(eV) | 4 | 5 | 7 | 10 | 15 | 20 | 45 |
|---|---|---|---|---|---|---|---|
| Statistical | 40 | 25 | 17 | 11 | 5 | 14 | 15 |
| Extrapolation | 25 | 10 | 10 | 10 | 10 | 12 | 25 |
| Elastic DCS | 7 | 7 | 5 | 4 | 4 | 4 | 2 |
| Normalization | 3 | 5 | 4 | 10 | 4 | 10 | 15 |
| Total (%) | 75 | 47 | 36 | 35 | 23 | 40 | 57 |

*e. Systematic errors.* Although the reproducibility of the energy-loss spectra is excellent, there could be systematic errors associated with the measured DCS's. However, our previously measured cross sections generally agree with those obtained by other investigators on other instruments where comparison can be made. We therefore believe that there is no significant contribution to the total error of a systematic nature.

The errors associated with the differential cross sections include the errors of the integral cross sections and an additional error which varies with angle. This additional error is estimated to be about 10% at the 10°–25° and 60°–80° ranges and about 5% for the 25°–60° range. At angles where the DCS's were obtained by extrapolation, the error could, of course, be considerably larger.

## IV. RESULTS AND DISCUSSION

### A. Differential Cross Sections

Table V and Figs. 8–10 summarize the DCS's for elastic scattering and for excitation to the $a\,^1\Delta_g$ and $b\,^1\Sigma_g^+$ states. The numbers inside the rectangular boxes in Table V are the measured values while those outside are the extrapolated values. In the case of the $X\,^3\Sigma_g^- \rightarrow b\,^1\Sigma_g^+$ transition, excitation of the $v' = 1$ level has been included, while for the $X\,^3\Sigma_g^- \rightarrow a\,^1\Delta_g$ transition, levels with $v' > 0$ are not appreciably populated (Table I) and were therefore neglected. The qualitative behavior of the DCS's for excitation of $a\,^1\Delta_g$ and $b\,^1\Sigma_g^+$ at 20- and 45-eV impact energies has been discussed in detail elsewhere.[22]

The elastic DCS decreases monotonically with increasing scattering angle in the 10°–90° range for all impact energies and it becomes steeper with increasing impact energy.

At all incident energies used in this study, the DCS for the $a\,^1\Delta_g$ excitation appears to peak in the forward direction, possesses a minimum in the 50°–80° range, and then increases again for large scattering angles.

The DCS measured for the excitation of the $b\,^1\Sigma_g^+$

state has an unusual behavior. For all incident energies studied, the DCS was found to decrease very rapidly as the scattering angle was decreased below 20°. Additional experiments were carried out to study the $b\,^1\Sigma_g^+/a\,^1\Delta_g$ ratio in the scattering angle range 3°–20° in order to determine just how fast the $b\,^1\Sigma_g^+$ DCS was falling. Special efforts were made to incorporate the proper EPLC because of the strong dependence on scattering angle. Although no measurements could be made at 0°, the DCS for excitation to this state at 0° is extremely small, or zero, based on extrapolation of these measurements in the 3°–20° range. The values of the DCS's near 0° shown in Fig. 10 are consequently somewhat uncertain and only represent the extrapolations used to obtain the integral cross sections.

At scattering angles greater than 20° the $b\,^1\Sigma_g^+$ DCS's possess maxima and minima whose locations are energy dependent. At 4-eV incident energy the DCS develops a maximum near 80° which shifts to less than 30° at 15 eV and becomes better defined.

The low-angle behavior of the $b\,^1\Sigma_g^+$ DCS shown in Fig. 10 seems to be the first observation of this type of angular dependence for an inelastic process in molecules. A dependence similar to this was predicted theoretically for the double excitation of ground-state He to the $(2p^2)^3P$ state by Becker and Dahler[23] and later confirmed experimentally by Simpson *et al.*[24] Fano then showed[25] that this transition in atomic He is one of a class of "parity-unfavored" transitions which in general have zero scattering amplitudes at 0° and 180°. The $b\,^1\Sigma_g^+ \rightarrow X\,^3\Sigma_g^-$ appears to fall into an analogous class for molecules and the details of this type of excitation are presently under study.

There are only two previous measurements of the DCS of the inelastic features reported here. Skerbele *et al.*[6] measured the intensity ratio, $I_a\,^1\Delta_g/I_{\text{elastic}}$, from 3° to 12° at 45-eV incident energy and found it to be constant and equal to $1.3\times10^{-4}$. Our ratio curve extrapolation (see Fig. 6) is in excellent agreement with this value. In their experiment, the $b\,^1\Sigma_g^+$ excitation was just barely detectable above the background at their largest scattering angle, which is consistent with the small-angle behavior of the DCS we measured for this excitation (Fig. 10).

Konishi *et al.*[9] determined DCS's for the $a\,^1\Delta_g$ and $b\,^1\Sigma_g^+$ states at 45°, 90°, and 145° scattering angles in the 20–70-eV impact energy range and found that the DCS's were the largest at 90°. This is in agreement with the conclusions one can draw from our measurements.

The unusual angular behavior of the DCS for excitation of the $b\,^1\Sigma_g^+$ state (a $\Sigma^- \rightarrow \Sigma^+$ transition) gives support to the reassignment of the 6.1-eV energy-loss feature in $O_2$ by Trajmar *et al.*[22] to the $X\,^3\Sigma_g^- \rightarrow c\,^1\Sigma_g^-$ transition. Previously, the 6.1-eV feature observed in electron-impact spectra was assumed to correspond to the $X\,^3\Sigma_g^- \rightarrow A\,^3\Sigma_u^+$ excitation. Since no drastic decrease of the measured DCS near zero scattering angle was found,[22] it is not believed to be a $\Sigma^- \rightarrow \Sigma^+$-type transition.

### B. Integral Cross Sections

Figure 11 shows the total cross sections for elastic scattering and for excitation of the $a\,^1\Delta_g$

TABLE V. Absolute electron-impact differential cross sections for elastic scattering and excitation of the $a\,^1\Delta_g$ and $b\,^1\Sigma_g^+$ states of $O_2$. The value for 10°–90° were obtained from experimental measurements while those outside represent the extrapolated values. The normalization of the data is described in the text.

| | $E_0$(eV) | | | | | | |
|---|---|---|---|---|---|---|---|
| θ (deg) | 4 | 5 | 7 | 10 | 15 | 20 | 45 |
| | $DCS_{\text{elastic}}$ ($10^{-16}$ cm$^2$/sr) | | | | | | |
| 0 | 0.942 | 1.04 | 1.799 | 5.481 | 6.671 | 6.058 | 14.240 |
| 10 | 0.920 | 0.937 | 1.606 | 3.350 | 4.255 | 4.503 | 7.690 |
| 20 | 0.897 | 0.914 | 1.371 | 2.253 | 2.718 | 3.193 | 3.759 |
| 30 | 0.875 | 0.823 | 1.232 | 1.675 | 1.883 | 2.210 | 1.766 |
| 40 | 0.852 | 0.816 | 1.124 | 1.309 | 1.286 | 1.515 | 0.854 |
| 50 | 0.807 | 0.765 | 1.017 | 1.035 | 0.879 | 0.999 | 0.416 |
| 60 | 0.754 | 0.741 | 0.878 | 0.834 | 0.637 | 0.708 | 0.234 |
| 70 | 0.686 | 0.674 | 0.728 | 0.670 | 0.453 | 0.499 | 0.148 |
| 80 | 0.603 | 0.596 | 0.610 | 0.566 | 0.373 | 0.369 | 0.105 |
| 90 | 0.505 | 0.518 | 0.493 | 0.487 | 0.322 | 0.274 | 0.079 |
| 100 | 0.422 | 0.460 | 0.402 | 0.414 | 0.282 | 0.217 | 0.061 |
| 120 | 0.332 | 0.380 | 0.294 | 0.335 | 0.233 | 0.154 | 0.041 |
| 140 | 0.279 | 0.333 | 0.225 | 0.286 | 0.206 | 0.120 | 0.031 |
| 160 | 0.249 | 0.298 | 0.179 | 0.262 | 0.184 | 0.098 | 0.025 |
| 180 | 0.226 | 0.274 | 0.148 | 0.238 | 0.171 | 0.082 | 0.020 |
| | $DCS_{a\,^1\Delta_g}$ ($10^{-19}$ cm$^2$/sr) | | | | | | |
| 0 | 6.94 | 5.18 | 9.64 | 14.0 | 9.77 | 8.92 | 1.77 |
| 10 | 5.66 | 5.72 | 8.89 | 11.0 | 7.25 | 5.24 | 1.48 |
| 20 | 4.42 | 5.62 | 8.14 | 8.34 | 4.95 | 3.19 | 1.20 |
| 30 | 3.66 | 5.01 | 7.39 | 6.27 | 3.34 | 2.78 | 0.97 |
| 40 | 3.24 | 4.38 | 6.64 | 5.12 | 2.64 | 2.91 | 0.83 |
| 50 | 3.07 | 3.50 | 6.32 | 4.46 | 2.62 | 3.15 | 0.73 |
| 60 | 3.25 | 4.36 | 6.32 | 4.26 | 2.76 | 3.32 | 0.67 |
| 70 | 3.92 | 4.64 | 6.64 | 4.26 | 3.12 | 3.36 | 0.68 |
| 80 | 4.70 | 5.03 | 7.50 | 4.38 | 3.50 | 3.36 | 0.83 |
| 90 | 5.09 | 5.40 | 7.93 | 4.63 | 3.77 | 3.29 | 0.94 |
| 100 | 5.39 | 5.72 | 8.09 | 4.87 | 3.91 | 3.19 | 1.03 |
| 120 | 5.66 | 5.83 | 7.82 | 5.05 | 3.93 | 2.82 | 1.05 |
| 140 | 5.53 | 5.53 | 7.07 | 4.93 | 3.77 | 2.33 | 0.97 |
| 160 | 5.28 | 5.08 | 6.21 | 4.63 | 3.51 | 1.88 | 0.82 |
| 180 | 4.98 | 4.54 | 5.35 | 4.26 | 3.17 | 1.47 | 0.66 |
| | $DCS_{b\,^1\Sigma_g^+}$($10^{-20}$ cm$^2$/sr) | | | | | | |
| 0 | ... | ... | ... | ... | ... | ... | ... |
| 10 | 4.05 | 3.13 | 5.89 | 6.09 | 8.28 | 6.71 | 1.14 |
| 20 | 6.64 | 5.80 | 10.5 | 10.4 | 15.0 | 10.2 | 2.11 |
| 30 | 9.40 | 7.91 | 16.1 | 14.0 | 14.5 | 10.6 | 2.53 |
| 40 | 12.0 | 1.16 | 21.4 | 14.0 | 12.2 | 10.4 | 2.53 |
| 50 | 14.1 | 1.39 | 24.1 | 12.8 | 10.8 | 10.7 | 2.22 |
| 60 | 15.6 | 1.58 | 24.6 | 11.0 | 10.1 | 11.6 | 2.11 |
| 70 | 16.0 | 1.67 | 23.6 | 10.7 | 9.78 | 12.7 | 2.28 |
| 80 | 16.2 | 1.67 | 21.4 | 10.7 | 9.43 | 13.2 | 2.73 |
| 90 | 15.9 | 1.65 | 18.2 | 11.3 | 9.09 | 13.0 | 3.25 |
| 100 | 15.4 | 1.58 | 16.2 | 11.6 | 8.86 | 12.4 | 3.42 |
| 120 | 13.4 | 1.39 | 13.9 | 11.7 | 8.05 | 10.3 | 3.36 |
| 140 | 11.3 | 1.14 | 12.4 | 11.3 | 7.25 | 8.02 | 3.02 |
| 160 | 9.32 | 0.893 | 11.2 | 10.7 | 6.33 | 5.98 | 2.51 |
| 180 | 7.29 | 0.696 | 10.7 | 9.74 | 5.41 | 4.34 | 1.99 |

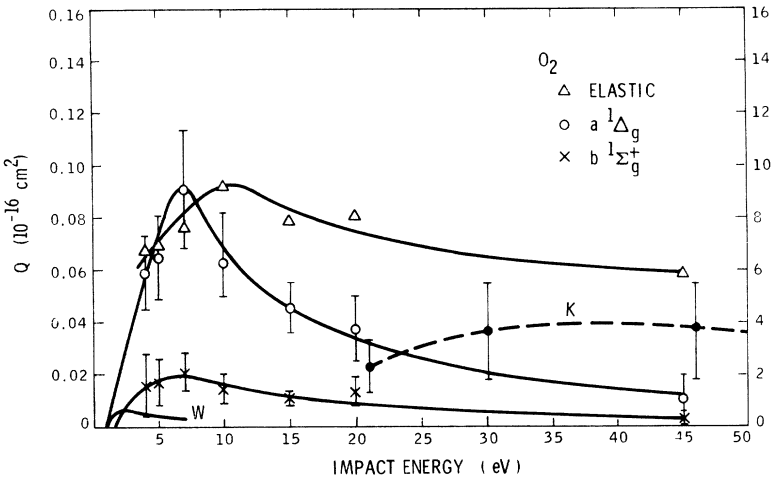


FIG. 11. Integral cross sections as a function of impact energy. The curves marked by W and K represent the integral cross sections for the excitation of the $a\,^1\Delta_g$ state as given by Watson *et al.* (Ref. 7) and Konishi *et al.* (Ref. 9).

and $b\,^1\Sigma_g^+$ states. The experimental values are indicated by different symbols with the corresponding error bars (see Tables III and IV for estimation of errors). The solid curves represent a best estimate of the shape of the cross sections which would pass through the data points. The left ordinate refers to the $a\,^1\Delta_g$ and $b\,^1\Sigma_g^+$ cross sections, while the right coordinate refers to the elastic one.

From an examination of the figure, one notes that these excitation cross sections reach their maximum at an incident energy of about 7 eV, which is a good deal farther above the threshold than is usual for "exchange" excitation processes.[26] It is quite possible that the somewhat unusual energy dependence found for these excitations is due to the relatively complicated structure of the ground state of $O_2$ (and possibly these low-lying excited states). That is, because of the fact that the ground state cannot be adequately represented by a single configuration, it is difficult to classify these excitations between two particular symmetry types even though the conventional term symbol notation implies that it is.

Also shown in the figure is the estimate for the $a\,^1\Delta_g$ excitation cross section which was made by Watson *et al.*[7] (curve marked by W). Their cross section is more than an order of magnitude smaller than ours at their respective maxima. The $b\,^1\Sigma_g^+$ integral cross section estimated by Watson *et al.*, although not shown in Fig. 11, is also correspondingly smaller than our measured cross section. The large cross sections deduced by Hake and Phelps[8] in the 1–2-eV energy range are consistent with our integral cross-section curves shown in Fig. 11. The somewhat unexpected magnitude and energy dependence of these excitation cross sections alters somewhat the previous interpretation of auroral and atmospheric phenomena involving $O_2$ as will be discussed elsewhere.[27]

Hasted proposed[5] to reconcile the observation of the strong 1.27-$\mu$ radiation in aurora (which requires $a\,^1\Delta_g$ cross sections of the order of $10^{-17}$ cm$^2$), with the low values found by Schulz and him, by proposing an excitation of the $a\,^1\Delta_g$ state from $X\,^3\Sigma_g^-(v'=1)$ via an $O_2^-$ state. Our results indicate that such a complicated mechanism may not be necessary to explain the present observations.

Konishi *et al.*[9] determined the integral cross sections for the $a\,^1\Delta_g$, $b\,^1\Sigma_g^+$, and 6.1-eV [assigned as $(A\,^3\Sigma_u^+ + C\,^3\Delta_u)$] excitations in the 20–70-eV impact energy range by measuring these inelastic and the elastic scattered signal intensities at 45°, 90°, and 135° scattering angles. They placed their cross sections on the absolute scale by normalizing the elastic differential cross sections to the total $e - O_2$ scattering cross sections of Sunshine *et al.*[19] Their cross sections are in agreement (within the combined experimental errors) with those of the present work at 20 and 45 eV. The curve marked by K in Fig. 11 gives their result for the excitation of the $a\,^1\Delta_g$ state. The agreement becomes better if their values are renormalized by taking into account the inelastic contributions to the total cross section in the manner discussed in Sec. III C. The apparent contradiction that their integral cross sections rise in the 20–45-eV region, while ours decrease, is explainable on the basis that the rise in their curve is within the errors of the measurement and decrease in our curve is just slightly outside of the estimated error. [Our cross section curves (Fig. 11) determined at lower energies seem to resolve this contradiction since the peaking of the cross sections at around 7 eV is clearly demonstrated.] The same remark applies also to the integral cross sections for the excitation of the $b\,^1\Sigma_g^+$ state.

The elastic scattering cross sections calculated by Fisk[21] are given in Table II for comparison. It should also be noted that this theoretical cross section, which is based on a semiempirical separable

electron-molecule interaction potential, agrees with the "measured" elastic cross section to within 13% for the energies used in this study.

ACKNOWLEDGMENTS

The authors thank Professor G. Schulz and Professor D. G. Truhlar for helpful discussions on certain aspects of this work and G. Steffensen for his help in processing the data. They also express their appreciation to Dr. J. K. Rice for his invaluable assistance in the development of the spectrum unfolding program.

*Work supported in part by the National Aeronautics and Space Administration under Contract No. NAS7-100.

†Conducted under U. S. A. F. SAMSO Contract No. F04701-70-C-0059.

[1]J. F. Noxon, J. Geophys. Res. 75, 1879 (1970).

[2]L. R. Megill, A. M. Despain, D. J. Baker, and K. D. Baker, J. Geophys. Res. 75, 4775 (1970).

[3]W. F. J. Evans, E. J. Llewellyn, J. C. Haslett, and L. R. Megill, J. Geophys. Res. 75, 6425 (1970).

[4]G. J. Schulz and J. T. Dowell, Phys. Rev. 128, 174 (1962).

[5]J. B. Hasted (unpublished). The authors are grateful to Professor Hasted for supplying them with a copy of his paper prior to publication.

[6]A. Skerbele, M. A. Dillon, and E. N. Lassettre, J. Chem. Phys. 49, 3543 (1968).

[7]C. E. Watson, V. A. Dulock, Jr., R. S. Stolarski, and A. E. S. Green, J. Geophys. Res. 72, 3961 (1967).

[8]R. D. Hake, Jr. and A. V. Phelps, Phys. Rev. 158, 70 (1967).

[9]A. Konishi, K. Wakiya, M. Yamamoto, and H. Suzuki, J. Phys. Soc. Japan 29, 526 (1970).

[10]D. C. Cartwright, W. Williams, and S. Trajmar, Bull. Am. Phys. Soc. 15, 1518 (1970).

[11]S. Trajmar, J. K. Rice, and A. Kuppermann, Jet Propulsion Laboratory Technical Memorandum 33-373, 1968 (unpublished).

[12]S. Trajmar, D. G. Truhlar, and J. K. Rice, J. Chem. Phys. 52, 4502 (1970).

[13]Neglect of rotational splittings is justified in this discussion because these are of the order of $10^{-3}$ eV which is nearly two orders of magnitude smaller than the instrumental resolution.

[14]R. N. Zare, University of California Radiation Laboratory Report No. 10925, 1963 (unpublished).

[15]D. Albritton, A. Schmeltakopf, and R. N. Zare, *Diatomic Intensity Factors* (Harper and Row, New York, to be published). We would like to thank these authors for providing the $O_2$ spectroscopic constants prior to publication.

[16]J. K. Rice, Ph. D. thesis (California Institute of Technology, 1968) (unpublished).

[17]D. C. Cartwright, S. Trajmar, and W. Williams (unpublished).

[18]A. Salop and H. H. Nakano, Phys. Rev. A 2, 127 (1970).

[19]G. Sunshine, B. B. Aubrey, and B. Benderson, Phys. Rev. 154, 1 (1967).

[20]L. J. Kieffer, *Bibliography of Low Energy Electron Collision Cross Section Data*, Natl. Bur. Std. Misc. Publ. 289 (U.S. GPO, Washington, D.C., 1967); G. E. Chamberlain and L. J. Kieffer, Natl. Bur. Std. Misc. Publ. 20 (U.S. GPO, Washington, D. C., 1969).

[21]J. B. Fiske, Phys. Rev. 49, 167 (1936). See also Yu. D. Oksyuk, Zh. Eksperim. i Teor. Fiz. 49, 1261 (1965) [Sov. Phys. JETP 22, 873 (1966)].

[22]S. Trajmar, W. Williams, and A. Kuppermann, J. Chem. Phys. (to be published).

[23]P. M. Becker and J. S. Dahler, Phys. Rev. Letters 10, 491 (1963).

[24]J. A. Simpson, S. R. Mielczarek, and J. W. Cooper, J. Opt. Soc. Am. 54, 269 (1964).

[25]U. Fano, Phys. Rev. 135, B863 (1964).

[26]B. L. Moiseiwitsch and S. J. Smith, Rev. Mod. Phys. 40, 238 (1968); L. J. Kieffer, JILA Information Center Report No. 7, 1969 (unpublished).

[27]D. C. Cartwright, W. Williams, and S. Trajmar (unpublished).

PHYSICAL REVIEW A VOLUME 4, NUMBER 4 OCTOBER 1971

# Eikonal Theory of Intermediate-Energy Electron-Atom Scattering*

Charles J. Joachain† and Marvin H. Mittleman‡
*Department of Physics, University of California, Berkeley, California* 94720
(Received 13 May 1971)

An eikonal theory of elastic electron-atom scattering in the region of intermediate energies is proposed. In addition to the effects of the static and polarization potentials, we also take into account the leading absorption corrections, using the equivalent-potential method. Detailed calculations are performed for elastic electron-helium scattering in the energy range 100–500 eV. Our results are in good agreement with the recent experimental data.

## I. INTRODUCTION

Present calculational techniques yield reliable results for electron-atom scattering processes when the relative incident energy is either low enough or sufficiently large with respect to typical target binding energies. In the former case only a few channels play an important role, so that close-cou-